THE JOURNAL OF PHYSICAL CHEMISTRY B

Article

pubs.acs.org/JPCB

Excitons in the LH3 Complexes from Purple Bacteria

Jevgenij Chmeliov,[†,‡] Egidijus Songaila,[†] Olga Rancova,[‡] Andrew Gall,[¶] Bruno Robert,[¶] Darius Abramavicius,[‡,§] and Leonas Valkunas*[,†,‡]

[†]Institute of Physics, Center for Physical Sciences and Technology, Gostauto 11, LT-01108 Vilnius, Lithuania

[‡]Department of Theoretical Physics, Vilnius University, Sauletekio Avenue 9, LT-10222 Vilnius, Lithuania

[¶]Institute of Biology and Technology of Saclay, CEA, UMR 8221 CNRS, University Paris Sud, CEA Saclay, 91191 Gif sur Yvette, France

[§]State Key Laboratory of Supramolecular Structure and Materials, Jilin University, 2699 Qianjin Street, Changchun 130012, People's Republic of China

Supporting Information

ABSTRACT: The noncovalently bound and structurally identical bacteriochlorophyll *a* chromophores in the peripheral light-harvesting complexes LH2 (B800−850) and LH3 (B800−820) from photosynthetic purple bacteria ensure the variability of the exciton spectra in the near-infrared (820−850 nm) wavelength region. As a result, the spectroscopic properties of the antenna complexes, such as positions of the maxima in the exciton absorption spectra, give rise to very efficient excitation transfer toward the reaction center. In this work, we investigated the possible molecular origin of the excitonically coupled B820 bacteriochlorophylls in LH3 using femtosecond transient absorption spectroscopy, deconvolution of steady-state absorption spectra, and modeling of the electrostatic intermolecular interactions using a charge density coupling approach. Compared to LH2, the upper excitonic level is red-shifted from 755 to 790 nm and is associated with an approximate 2-fold decrease of B820 intrapigment coupling. The absorption properties of LH3 cannot be reproduced by only changing the B850 site energy but also require a different scaling factor to be used to calculate interpigment couplings and a change of histidine protonation state. Several protonation patterns for distinct amino acid groups are presented, giving values of 162−173 cm^{-1} at 100 K for the intradimer resonance interaction in the B820 ring.

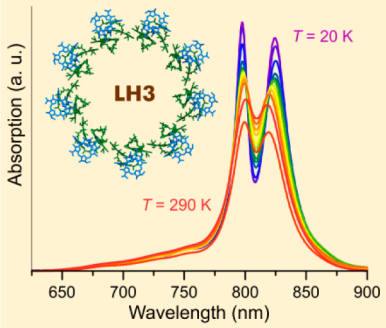

1. INTRODUCTION

In photosynthetic organisms, the light-harvesting antenna system enhances their capacity to absorb photons and allows photosynthesis to operate efficiently over a wide range of light intensities and wavelengths. After absorption, the resulting excitation energy is transferred from the light-harvesting antenna to the reaction center, where it is stabilized as a chemical potential.[1] In many photosynthetic purple bacteria, the light-harvesting system is comprised of two types of antenna complexes, the core LH1 complexes, which are situated in the vicinity of the reaction centers, and the peripheral LH2 complexes surrounding them.[2] The elucidation of the structure of the LH2 complex from the purple bacterium *Rhodoblastus* (*Rbl.*) *acidophilus*[3] has provided a visual framework to describe these processes, both experimentally and theoretically. This LH2 complex is a circular structure comprised of nine copies of the minimal unit that contains two short transmembrane-spanning polypeptides, designated α and β. Each minimal unit, herein termed the α/β-dimer, binds three bacteriochlorophyll (BChl) molecules; two are embedded deep in the hydrophobic phase of the membrane, while the third one is located more toward the N-terminal domain. The former BChl molecules are in close contact and exhibit strong excitonic coupling. Their long-wavelength electronic transitions are responsible for the absorption at 850 nm (the so-called B850 band) of the complex. The absorption at 800 nm (the B800 band) arises from the remaining nine weakly coupled BChl molecules. Each α/β-dimer also binds one all-trans carotenoid molecule.

Due to their well-defined circular symmetry, the LH2 complexes offer a unique opportunity to compare experimental spectroscopic observations with theoretical predictions. In order to accurately describe the electronic absorption properties of these antenna complexes in terms of the exciton model, the static disorder of pigment site energies, as well as the dynamic disorder induced by the coupling of the electronic excitations to intra- and intermolecular vibrations and phonons caused by collective vibrations of the surrounding protein, must be taken into account.[4−9] Exciton model parameters, in particular, the resonance intermolecular interaction between the nearest B850 pigments, are essential factors for an accurate description of the electronic properties in forming the "ring"

Special Issue: Rienk van Grondelle Festschrift

Received: January 8, 2013
Revised: February 28, 2013

   dx.doi.org/10.1021/jp400239z | *J. Phys. Chem. B* XXXX, XXX, XXX−XXX

structures. The resonance interaction between the nearest pigment molecules was extracted from the simulation of the experimental observations. Its value, however, varies between 300 and 420 cm^{-1} depending on whether it was determined from the analysis of low-temperature absorption,[10] fluorescence,[11] or hole-burning experiments.[12] Slightly smaller values have been accessed from the quantum chemistry calculations[13,14] by using a collective electronic oscillator approach[15] and by the electrostatic modeling of the Frenkel exciton Hamiltonian,[16] which demonstrated a dominating role of the protein solvation in determining the intermolecular interaction. These values of the resonance interactions in LH2, as well as their dependencies on the approaches used for their determination, have been extensively discussed.[17] The most reliable values of this parameter were defined as a measure of the exciton energy bandwidth. Low-temperature (1.2 K) fluorescence−excitation measurements on LH2 complexes from *Rbl. acidophilus* led to a value of 250 cm^{-1} for the resonance interaction,[18] which was later determined to be temperature-dependent.[19]

Strains 7750 and 7050 of *Rbl. acidophilus* are able to synthesize a spectrally different type of peripheral light-harvesting complex, which is often called LH3.[20−22] The main difference in the BChl absorption properties is the position of the longest BChl−Q_y transitions; it is located at ∼820 nm instead of at ∼850 nm. The spectral change, which is not unique to *Rbl. acidophilus*, was determined to tightly correlate with specific changes of the primary sequence of the α-apoproteins[23] and was later confirmed by site-directed mutagenesis studies.[24] In the present work, our aim was to determine the possible origin of the spectral shift in LH3 complexes and the parameters of the exciton spectra of their lower-energy absorption transition, both from experimental studies and theoretical modeling.

2. MATERIALS AND METHODS

Rbl. acidophilus strain 7750 cells, adapted to low-light conditions, were harvested in midlog phase, the membranes were prepared, the light-harvesting complexes were isolated by a sucrose gradient centrifugation, and LH3 were purified essentially using methods previously described.[20,25,26] The final composition of the LH3 samples used for spectroscopic studies was in 20 mM Tris-Cl (pH 8.5) buffer containing 0.1% *N,N*-dimethyldodecylamine-*N*-oxide (LDAO) (w/v) (Fluka).

The temperature dependence of the absorption spectra was collected using a Varian Cary E5 double beam scanning spectrophotometer on samples containing 60% (v/v) glycerol (final concentration). The temperature of the samples was maintained by a helium flow cryostat (TBT, Sassenage, France). Absorption spectra were measured after a delay of 15 min to allow temperature equilibration of the sample. Spectra were corrected for the background absorption as determined at each temperature using a cuvette filled with the Tris-Cl/glycerol buffer. Spectral data mining was performed by using the MATLAB software package.

For pump−probe measurements, steady-state absorption spectra of LH3 samples were recorded using a Perkin-Elmer Lambda 950 spectrometer. Transient absorption was recorded by means of the conventional femtosecond absorption pump−probe spectroscopy. The spectrometer was based on the amplified femtosecond Ti:Sapphire laser Quantronix *Integra-C* generating 130 fs duration pulses at 805 nm (1.55 eV) at a 1 kHz repetition rate. Tunable wavelength excitation was provided by a parametric generator TOPAS C. Probing was ensured by a white light continuum generated by illuminating a 2 mm thick sapphire plate. The excitation beam was focused on a spot of ∼500 μm in diameter, and the probe beam diameter was kept at ∼300 μm. In order to avoid the influence of exciton−exciton annihilation on the transient absorption kinetics, excitation intensity below the annihilation threshold was used. The optical density of the sample at 820 nm was 0.40 cm^{-1}.

3. EXPERIMENTAL RESULTS

The near-infrared wavelength region of the absorption spectra of the LH2 and LH3 complexes from *Rbl. acidophilus*, normalized at the Q_x absorption band of the BChl molecules (around 590 nm), is displayed in Figure 1. In this region, both

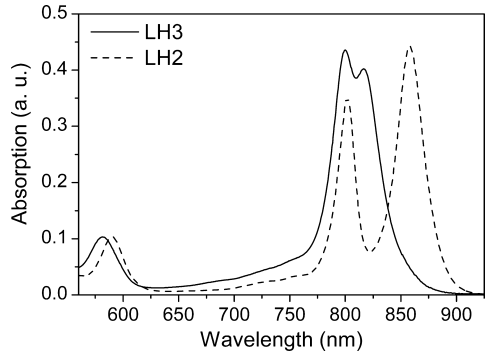

Figure 1. Room-temperature absorption spectra of LH2 (dotted line) and LH3 (solid line) complexes from *Rbl. acidophilus*.

pigment−protein complexes have two main BChl−Q_y absorption bands, one centered at ∼800 nm and another situated at ∼820 nm (LH3) or ∼850 nm (LH2). Compared to LH2, the difference in the relative peak intensities of the two absorption bands is due to the overlap of the two BChl−Q_y transitions. As in the case of the LH2 complexes,[5−7] this part of the absorption spectrum depends on temperature (Figure 2). The absorption band located at 800 nm (at room temperature) slightly shifts to the red (i.e., to lower energies) as the

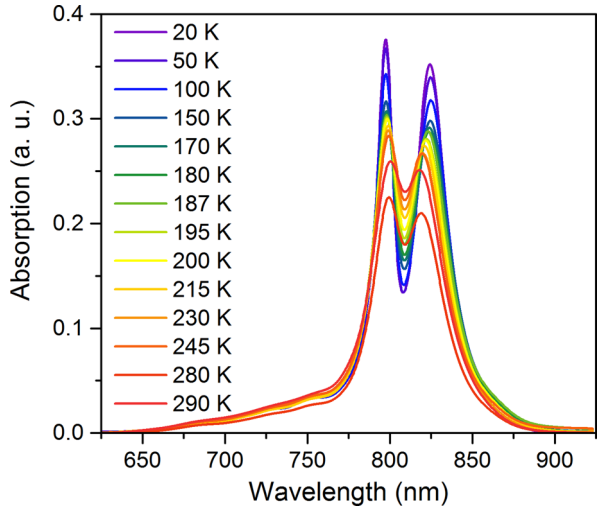

Figure 2. Near-infrared absorption spectra of LH3 complexes from *Rbl. acidophilus* measured at different temperatures, ranging from 20 to 290 K.

dx.doi.org/10.1021/jp400239z | *J. Phys. Chem. B* XXXX, XXX, XXX−XXX

temperature increases, while at the same time, the peak centered at 820 nm essentially shifts to the bluer wavelengths. The widths of both bands increase with temperature.

In order to determine the exciton structure of the ring corresponding to the absorption at 820 nm, the excitation transient spectra were analyzed using the approach recently developed for LH2.[27] The idea behind these experiments is that direct excitation in the B820 manifold should result in an instantaneous bleaching of the B820 band, while exciting in the B800 absorption ring should result in a delayed bleaching of the absorption due to the slower excitation energy transfer from the B800 ring to the B820 one. The kinetics corresponding to the excitation transient spectra can be described by means of the following expression[27]

$$\Delta A(\lambda, t) = F(\lambda) + S(\lambda)[1 - e^{-t/\tau}] \quad (1)$$

where λ is the excitation wavelength, F determines the amplitude of the fast kinetics, and S is the amplitude of the slow kinetics with the characteristic time τ. Strictly speaking, the instantaneous component should reflect the excitation relaxation through the excited levels of the B820 ring during the processes faster than the time resolution of our setup (130 fs). The results obtained by fitting the experimental data are presented in Figure S1 in the Supporting Information, and the calculated ratio of the fast component to the total intensity is shown in Figure 3. Contrary to what is observed in LH2 complexes,[27] this ratio is almost insensitive to the excitation wavelength, and thus, we cannot distinguish any specific band that can be attributed to the upper Davydov component of the exciton band of the B820 ring.

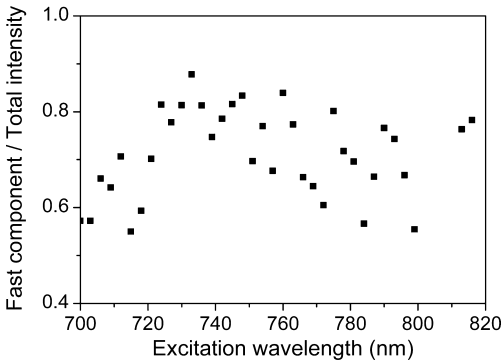

Figure 3. Relative intensity of the fast decay component to the whole amplitude of the excitation transient spectra as a function of excitation wavelength.

4. MODELING OF THE ABSORPTION SPECTRUM OF THE LH3 COMPLEXES

4.1. Temperature Dependence of the Absorption Spectra. Our experimental results indicate that the upper excitonic band of the 18 BChls in the B820 is very weak and, more importantly, that it overlaps with the B800 absorption band. In order to discriminate between the optical transitions that correspond to the B800 and B820 bands, we analyzed a series of absorption spectra of LH3 complexes measured at different temperatures from 290 to 20 K (Figure 2). For this purpose, we used the self-modeling curve resolution method described previously.[19]

First, we decomposed the absorption spectrum of the LH3 complexes to the sum of a series of Gaussian peaks (12 Gaussians were required to reproduce all of the details of each absorption spectrum, while increasing this number did not result in any noticeable improvement of the fits). This number of spectral components required to reproduce the absorption spectra may be considered to be related to the number of excitonic and vibronic transitions of the BChl molecules from the B800 and B820 rings. Next, we assigned all three Gaussian peaks located around 800 nm to the B800 absorption band, while the rest were considered to belong to the B820 transition. In the case of the LH2 complexes,[19] such an assignment of the Gaussian peaks was justified by the experimental evidence that that upper excitonic band in those complexes was located in the region between 750 and 770 nm.[27] However, the transient absorption kinetics of the LH3 complexes, measured in the present work, did not reveal any obvious peaks belonging to the B820 ring. This may indicate that that the upper exciton subband might be shifted to the red (when compared to LH2) and located at ~800 nm. Therefore, we also considered that possibility during the modeling process.

We used all of the determined Gaussian peaks as the initial spectral constituents in the iterative process to obtain 12 spectral shapes that, upon multiplication by some temperature-dependent amplitudes, reproduced all of the experimentally obtained absorption spectra measured at different temperatures. Mathematically, this can be expressed as a decomposition of the initial data matrix $\mathbf{Y}$ of dimensions $m \times n$ (representing the absorption spectra at m wavelength points and measured for n different temperatures) to the product of two matrices with an added matrix of residuals

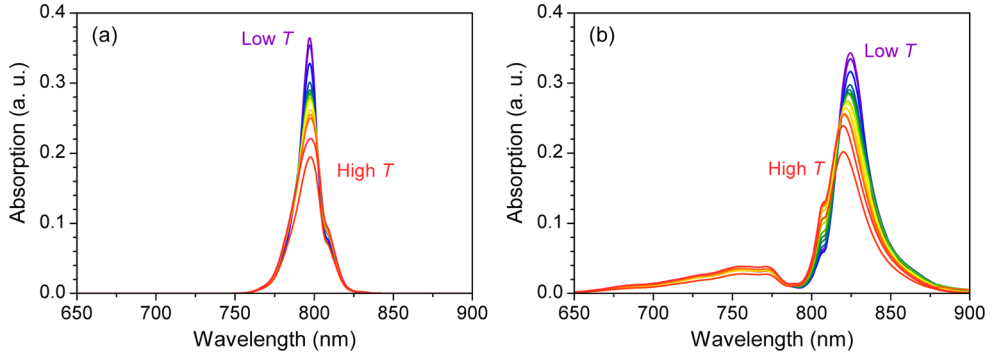

Figure 4. Deconvoluted absorption spectra of B800 (a) and B820 (b) bands with all three Gaussians centered at around 800 nm initially ascribed to B800. Various colors correspond to the same temperatures as those in Figure 2.

dx.doi.org/10.1021/jp400239z | J. Phys. Chem. B XXXX, XXX, XXX−XXX

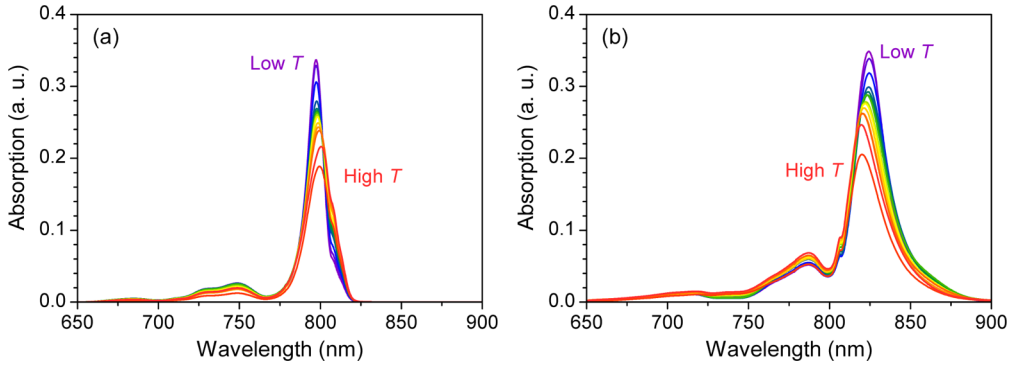

Figure 5. Deconvoluted absorption spectra of B800 (a) and B820 (b) bands with one of three Gaussians centered at around 800 nm initially ascribed to B820. Various colors correspond to the same temperatures as those in Figure 2.

$$\mathbf{Y} = \mathbf{S}\cdot\mathbf{W} + \mathbf{E} \quad (2)$$

where **S** is a matrix of dimensions $m \times k$ with columns corresponding to k spectral components for m already chosen wavelengths (in our case, $k = 12$); **W** determines the matrix of dimensions $k \times n$, where k rows are filled with the weighting factors for the above-mentioned spectral constituents at n different temperatures. Matrix **E** represents the residual matrix, which is reduced to a minimal value during the iteration process.

In general, such decomposition is not unique, but uniqueness can be achieved by imposing that the B820 band arises from 18 BChls whereas only 9 BChls are responsible for the B800 band. Therefore the ratio of the integral absorption of these transitions should be close to 2. Keeping in mind this additional constraint, we initially ascribed the Gaussians to either B800 or B820 bands in such a way that even before performing the factorization algorithm, the ratio of the integral absorption of both bands was as close to the desired value of 2 as possible. Consequently, the decomposition procedure converged to a unique result. The obtained spectral components, their temperature-dependent amplitudes, and the relative errors of the deconvoluted spectra are presented in the Supporting Information. The deconvoluted absorption spectra of the B800 and B820 bands are shown in Figure 4 (initially ascribing the whole intensity around 800 nm to the B800 transition) and Figure 5 (initially attributing one Gaussian component at 800 nm to the B820 band).

In both cases, we obtained the decompositions of the B820 absorption bands that are very similar to those obtained for LH2,[19] while the bandwidths of the B800 bands are notably narrower. This indicates that the structural variations between LH2 and LH3 antenna complexes result not only in the spectral shift of the B850/B820 bands, but also the different widths of the B800 band. Furthermore, when compared to LH2, LH3 complexes manifest a pronounced temperature-dependent intensity variation of the near-infrared absorption spectrum as well as a smaller shift of the B820 absorption band.

When all the spectral components centered at 800 nm are initially attributed to the B800 band, the demand to maintain the ratio of the integral absorption of the B820 and B800 bands equal to 2 attributes the whole blue region of the LH3 spectrum solely to the B820 ring. If true, that should have resulted in a large fraction of instantaneous bleaching when exciting the complexes at around 750 nm, which is not observed in the transient absorption data (Figure 3). On the other hand, if we initially assign one Gaussian peak located at around 800 nm to the B820 band, the B800 transition exhibits a slightly narrower bandwidth, and the mentioned requirement for the ratio of the integral absorption of the B820 and B800 bands forces some of the additional peaks in the blue region of the spectrum (of possibly vibronic nature) to be attributed to the B800 band. As a result, the relative absorption intensities of the B820 and B800 rings are reasonably constant in this blue spectral region, in accord with the femtosecond data displayed in Figure 3.

Once the spectral components attributed to B800 band have been removed, the excitonic transitions of the B820 band can be clearly distinguished. The maximal positions of the excitonic transitions at different temperatures, obtained for the two discussed cases, are presented in Figure 6.

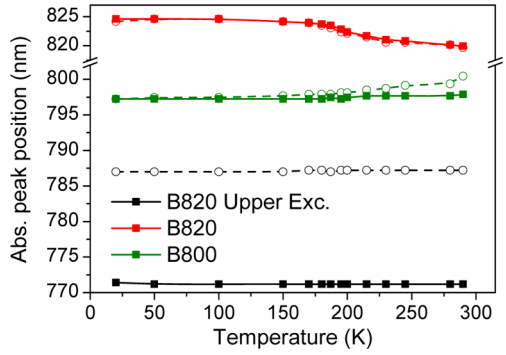

Figure 6. Temperature dependence of the absorption maxima ascribed to the BChl-800 and the excitonic transitions of the BChl-820 molecules in LH3. The solid and dashed lines correspond to the deconvoluted spectra presented in Figures 4 and 5, respectively.

As compared to the LH2 complex from *Rbl. acidophilus*, not only has the lower excitonic subband of LH3 significantly shifted to a shorter wavelength (820 nm vs 850 nm) but also the energy of the upper excitonic level has red-shifted (771 or 787 nm instead of 755 nm for LH2). Such a result indicates an approximate 2-fold decrease of both the difference between the corresponding energy levels as well as coupling between strongly interacting BChls in LH3 as compared with that in LH2 complexes. However, both decompositions exhibit similar errors, and because (unlike with LH2 complexes[19]) we can rely only on negative indications provided by the transient absorption data for the position of the upper Davydov component of the exciton band corresponding to the B820 ring, an additional investigation of the exciton spectra should be

dx.doi.org/10.1021/jp400239z | J. Phys. Chem. B XXXX, XXX, XXX−XXX

Table 1. Parameters Used to Model Absorption Spectra

	model I	model II	model III
protein charge layout	Glu negative; His13 and -15 positive; His37 positive	Glu, His13 and -15 neutral; His37 positive	Glu, His13 and -15 neutral; His37 neutral
scaling factor f	0.60	0.60	0.62
system−bath coupling factor	1.2	1.2	1
Gaussian diagonal disorder	30 cm^{-1} (B800)	30 cm^{-1} (B800)	37 cm^{-1} (B800)
	210 cm^{-1} (B820)	210 cm^{-1} (B820)	185 cm^{-1} (B820)
difference between mean site energies of B800 and B820	216 cm^{-1}	212 cm^{-1}	233 cm^{-1}
difference between mean site energies of B820α and B820β	212 cm^{-1}	178 cm^{-1}	438 cm^{-1}
obtained nearest-neighbor excitonic coupling	162 cm^{-1}	162 cm^{-1}	173 cm^{-1}

carried out in order to choose, which solution reflects the physical properties of LH3 complexes.

4.2. Calculation of the Frenkel Exciton Hamiltonian from the Electrostatic Interactions. The absorption spectrum of photosynthetic antenna complexes is usually defined in terms of the Frenkel exciton Hamiltonian in the representation of the pigment excitations[4−7,28−31]

$$\hat{H} = \sum_{m} E_m \hat{B}_m^{\dagger}\hat{B}_m + \sum_{\substack{m,n \\ m\neq n}} V_{mn}\hat{B}_m^{\dagger}\hat{B}_n \tag{3}$$

where E_m is the excitation site energy of the mth pigment, V_{mn} is the energy of the interpigment resonance interaction, $\hat{B}_m^{\dagger}$ is an excitation creation operator for the mth pigment, and $\hat{B}_m$ is a hermitian-conjugate annihilation operator.

The available crystallographic data of the LH3 complex from the *Rbl. acidophilus* strain 7050[32] provides the possibility to directly estimate the values of the elements of the Frenkel exciton Hamiltonian by taking into account the electrostatic interactions within the complex. The later can be defined as the Coulomb couplings between the partial charges assigned to the atoms of the pigments and the protein molecules of the photosynthetic complex.[33−37] For this, we use the charge density coupling (CDC) method,[34] which has been developed to calculate the shift of the site energies in the protein surrounding,[33−37] and the transition charge from electrostatic potential (TrEsp) method[35] to compute the excitonic couplings from the electrostatic interactions between pigments. The electrostatic background, responsible for the site energies of the pigments, arises from the electrostatic potential created by the atomic partial charges of the molecules not involved in the electronic transition (such as carotenoids in their ground state as well as the protein backbone and side chains with their dipole moments) and the polarization charges formed by hydrogen bonds (H-bonds) to the pigments.

The essential difference between our approach and the original CDC method lies in the determination of the atomic partial charges of the protein. In the original CDC method, the protonation states of the titratable residues are either assumed to be standard[34] (as in a solution at pH 7) or obtained from the calculations of the electrostatic energy.[38] However, we consider the protonation pattern of the complex as a tunable parameter based on the standard protonation states. We also assume the dielectric constant being just responsible for the effective screening and treat it as a fitting parameter. Thus, in our approach, we search for the best set of parameters generating an appropriate Frenkel exciton Hamiltonian and use the experimentally observed spectra of the photosynthetic complex as a benchmark. This approach has been already used to model the linear absorption and circular dichroism spectra of the LH2 complexes.[16]

As stated in the introduction, the most obvious difference between LH2 and LH3 is a ∼30 nm shift of one of the BChl−Q_y absorption bands. The origin of this absorption shift was first related to the differences in the primary sequences[23] that strongly suggested that specific residues, which are capable of forming H-bonds, were somehow involved. This was confirmed when LH3-like LH2 mutants of *Rhodobacter* (*Rba.*) *sphearoides* were created using single/double site mutagenesis[24] and the H-bonding network was verified by Raman spectroscopy,[39] in preresonance with the B850/820 pigments. In parallel, the importance of H-bond formation on the electronic properties of the B850/820 band was established in a systematic study of naturally occurring LH2 complexes and their LH3 counterparts.[40] Finally, the precise nature of the connectivity of the H-bonding network was refined upon the elucidation of the three-dimensional structures of LH2[3] and LH3.[32] The site-directed mutants of *Rba. sphearoides* resulted in a maximum 26 nm blue shift of the B850 band absorption spectrum at 77 K,[3] and the downshift of the energy sites of BChl-850 was experimentally determined to be ∼100 cm^{-1}.[41] This value was obtained in a recent simulation study of LH2, demonstrating the legitimacy of the calculations.[16]

Keeping the above in mind, we first assume that the difference between the LH2 and LH3 is solely due to a different H-bond network, and the absorption spectrum of the LH3 complex can be modeled by applying the technique developed for LH2.[16] The obtained site energies are very similar to the ones of LH2 except for the 100 cm^{-1} downshift of the site energies of the B820 pigments due to the absence of the above-mentioned H-bonds. However, the peak positions in the simulated LH3 absorption spectrum were significantly shifted as compared with the experiment; in the modeled absorption spectrum, the distance between the peaks' maxima was approximately 54 nm, which is almost twice the value obtained from the experimental observation (29 nm at 100 K). Therefore, besides the H-bonding pattern, additional differences must exist in the modeled system to account for absorption properties of the LH3 complexes.

In order to achieve a better description of the spectroscopic properties of LH3, we kept the same effective dielectric constant and atomic partial charge distributions, representing the potential of the ground and first excited states of the pigments, as in the previous LH2 model;[16] however, we tuned other microscopic parameters of our model while treating the experimental absorption spectrum at 100 K as a benchmark. With such an approach, we found three possible sets of parameters (layouts of the atomic partial charges within the

dx.doi.org/10.1021/jp400239z | J. Phys. Chem. B XXXX, XXX, XXX−XXX

pigment−protein complex) for electrostatic calculations of the Frenkel exciton Hamiltonian matrix elements. These parameters are summarized in Table 1.

First, we used the set of parameters obtained for the LH2 complex[16] and based on the standard protonation states of amino acids while tuning the protonation states of the side chains of the histidine (His) residues (model I in Table 1). The imidazole side chains have several protonation possibilities, which are, in the protein context, very sensitive to the nearest surrounding: they can be doubly protonated and positively charged, singly protonated and neutral, or doubly deprotonated and negatively charged.[42] There are five histidine amino acids per symmetric unit in LH2:[43] B850 BChl ligands α-His31 and β-His30, β-His12 close to the cytoplasmic side of the complex, and α-His37 and β-His41 on its periplasmic side (following the residue notation in the PDB file). In LH3,[23] there are analogous B820 ligands α-His31 and β-His31, two histidines close to the cytoplasmic side of the complex (β-His13 and -15), and α-His37 on the periplasmic side (see Figure 7). In the model of

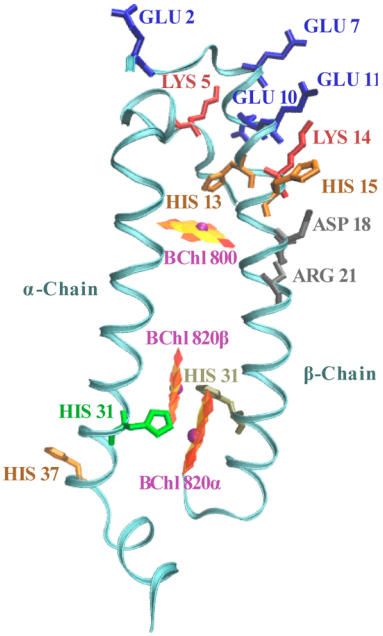

Figure 7. The symmetric unit of the LH3 complex (C-terminal parts of the polypeptides are missing in the structural data). The titratable residues are depicted explicitly: Arg−Asp neutral pair, gray; Glu, blue; Lys, red; His (not BChl ligands), orange; α-His31, green; β-His31, tan; BChl, yellow−orange cartoons with a purple central Mg atom. Created with VMD.[44]

LH2, in order to compensate for the effect of the negatively charged glutamic acid (Glu) side chains on the cytoplasmic side of the complex, we set β-His12 to be doubly protonated and positively charged. We also assumed α-His37 and β-His41 to be singly protonated and neutral, the ligand α-His31 to be neutral, and the ligand β-His30 to be deprotonated and negative. This negative ligand produced approximately up to 300 cm^{-1} splitting between the site energies of the α- and β-bond pigments in the B850 ring.

The protonation states deduced from our modeling and the resulting charges found on the His30 ligand may just reflect unusual charge repartition on its imidazole side chain, which would cause almost totally negative charge close to the BChl pigment. Otherwise, taking the standard charge layout of the protein, the calculated site energies of the BChls from the B820 (B850) ring appear to be approximately equal. We approach the issue of the charge repartition within the bacteriochlorophyll−imidazole complexes in the Discussion section.

Following this model for LH2 and seeking to reproduce the absorption spectrum of the LH3 complexes, we suggest histidines His13 and -15 on the cytoplasmic side to be positively charged, ligands α-His31 being neutral and β-His31 being negative. Unlike in the LH2 model, we set α-His37 as doubly protonated and positively charged. To justify the presence of both negatively and positively charged histidines on the periplasmic side of the pigment−protein complex, we emphasize that negatively charged His31 belongs to the β-polypeptide and is located close to the outer side of the overall cylindrical structure of LH3, whereas the positive His37 belongs to the α-polypeptide and is situated in the inner side of the cylinder close to the membrane interface.

We also investigated the possibility for glutamic and aspartic acids in the membranes and inside of the proteins to be protonated and thus neutral. In LH3 (as well as in LH2) complexes of *Rbl. acidophilus*, all glutamic acids are on the cytoplasmic side of the β-polypeptides. The assumption that the glutamic acid side chains are protonated and neutral leads to the conclusion that the histidine residues on the cytoplasmic side (namely His13 and -15) are neutral as well. Then, we checked two possibilities for the protonation state of the remaining nonligating histidine residue His37 (being either positive or neutral), thus obtaining two more possible charge layouts within the LH3 complex, which are summarized in Table 1 as model II and model III, respectively.

As a result, we have selected three possible sets of parameters for CDC calculations of the site energy shifts of the pigments. By taking into account the electrostatic interactions with the discussed patterns of the atomic partial charges within the LH3 complex, these parameters allowed us to determine the necessary diagonal elements of the Frenkel exciton Hamiltonian (the site energies E_m in eq 3). However, as discussed below, other adjustable parameters play equally or even more important roles while modeling the absorption spectra.

The next step was to calculate the off-diagonal elements of the Frenkel exciton Hamiltonian, that is, the interpigment excitonic couplings V_{mn} defined in eq 3. Within the TrEsp approach,[35] we assumed that these couplings depend only on (i) the atomic partial charges reproducing the transition potential of the BChl molecules, (ii) interatomic distances between these charges, and (iii) the optical dielectric constant of the environment. In our model, we took the fixed positions of the atoms, defined in the crystallographic data,[32] and the partial charge sets of the Q_y transition of the BChl *a* molecules, as obtained by Madjet et al.[35] by using the TDDFT/B3LYP method. The calculated partial charges describe the transition potential of the BChl qualitatively, and their absolute magnitudes have to be renormalized to some observable. For this purpose, we applied the factor f to rescale the set of the calculated transition partial charges. However, the magnitude of the transition dipole moment of BChls depends on the solvent and on the interpretation methods. Thus, for the BChl *a* molecule, one can find values of 6.1 or 6.6 D,[45] as well as 6.3 D.[46] Therefore, we have some freedom to adjust the scaling factor f. Our argument for this adjustment is not the value of the dipole moment of the BChl molecule but the correct reproduction of the experimental absorption spectrum. For simplicity, we set the optical dielectric constant equal to unity

dx.doi.org/10.1021/jp400239z | J. Phys. Chem. B XXXX, XXX, XXX−XXX

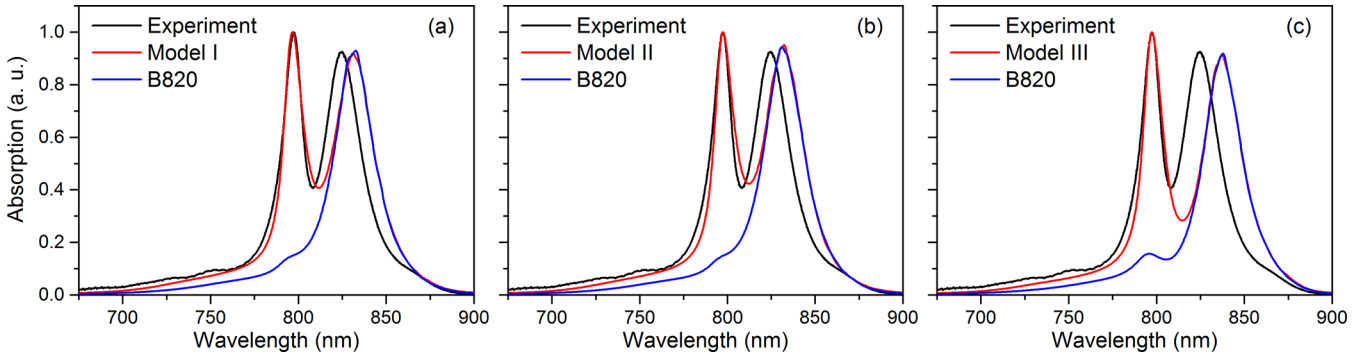

Figure 8. Experimental and modeled absorption spectra of the LH3 complex at 100 K calculated for three different parameter sets (the maximum of the B800 band was normalized to 1).

and then treated the scaling factor of the calculated atomic partial charges, *f*, as some quantity representing the dielectric effect of the environment as well.

In order to determine the excitonic couplings between the pigments within the complex, we again started with the same scaling factor $f = 0.81$ as that in the case of LH2.[16] However, by applying it to the LH3 absorption spectrum, we obtained a B820 peak that was too strong, too narrow, and too far shifted to the red side. Therefore, by varying the value of *f*, we had to adjust the strength of the excitonic couplings between the dimeric pigments from the B820 ring. We realized that the values of *f* lying in the range of 0.60−0.62, depending on the three possible models for the site-energies described above (see Table 1), reproduced the absorption spectrum of LH3 in the best way. These values are rather small compared, for instance, with the scaling factor $f = 0.732$, which gives the transition dipole moment of 6.3 D[46] when applied to the calculated atomic partial charges of BChls.[35] The possible interpretation of this scaling factor is given in the Discussion section.

The matrix elements of the calculated Hamiltonian are presented in Table S1 in the Supporting Information. Compared with the model used for LH2 calculations,[16] the site energies of the pigments are shifted by the same value in order to compensate for the effect of the spectral densities used in the calculations, as described below. It is worthwhile to mention that the nearest-neighbor coupling of the pigments in the B820 ring is 162 cm^{-1} in the first and second models and 173 cm^{-1} in the third one, which is significantly smaller than the value of ∼273 cm^{-1} obtained from the LH2 modeling.[16] This change is the result of the different scaling factor applied to the calculated transition atomic partial charges as well as altered distances between the atoms of the pigments.

4.3. Calculation of the Absorption Spectrum. Having fully defined the Hamiltonian in eq 3 and implementing the methods already described,[30,47] the simulation of the absorption spectrum was performed in the same way as in the case of LH2.[16] In order to reproduce the measured absorption spectrum, the spectral densities of the pigments and the inhomogeneous disorder parameters were adjusted. As the high-energy wing of the spectrum is of particular interest in the present research, we have chosen not to use the spectral density obtained for LH2[48] as it lacks high-frequency features. The spectral densities of the BChl environment in LH2 were studied using the molecular dynamics simulations combined with quantum chemistry methods,[49] and a range of high-frequency modes was found to contribute to the fluctuations. However, to simplify calculations, in our simulations, instead of employing multipeak spectral density,[49] we used a broad spectrum of a damped harmonic oscillator[50]

$$C''(\omega) = \frac{2\sqrt{2}\,\lambda\omega\omega_0^2\gamma}{(\omega^2 - \omega_0^2)^2 + 2\gamma^2\omega^2} \quad (4)$$

with the following parameters adjusted to represent equally well the absorption spectra of both LH2 and LH3 complexes: $\gamma = 663.6$ ps^{-1}, $\lambda = 480$, and $\omega_0 = 1300$ cm^{-1}. In order to bring our three models into agreement with the experimental spectrum, we used different dimensionless system−bath coupling factors, 1.2 in the first and second models and 1.0 in the third one (see Table 1).

The uncorrelated Gaussian diagonal disorder was also adjusted for all the three different models and was assumed to be equal to $\sigma_{B800} = 30$ cm^{-1} and $\sigma_{B820} = 210$ cm^{-1} in the first two models, and $\sigma_{B800} = 37$ cm^{-1} and $\sigma_{B820} = 185$ cm^{-1} in the third one. All of the calculated spectra were averaged over 5000 realizations. The calculated absorption spectra at 100 K are presented in Figure 8 and exhibit rather good agreement with the experimental one.

The modeled B820 band is slightly shifted to lower energies compared with the experimental one. However, this shift could be due to the fact that the residues close to C-termini of the proteins within the complex are not resolved in the LH3 crystal structure,[32] and therefore, their influence was ignored during the calculations. The exact positions of the high-frequency components in the LH3 absorption spectrum are also not reproduced, but the qualitative agreement with the experimental one and the overall shape of the modeled spectra are rather good.

In order to determine the origin of the high-energy features of the absorption spectrum and seeking to distinguish between the upper excitonic component of the B820 band and possible vibronic components arising from the spectral density function used in the calculations, we calculated the impact of the pigments from the B820 ring on the absorption spectrum separately. The results are presented in Figure 8 together with the total calculated spectrum (the amplitudes of the B820 spectra were normalized to fit the total modeled spectra). Now, it is clearly seen that in all of our models, the upper excitonic component of the dimeric B820 ring is hidden under the B800 band. The upper excitonic component is most prominent in the third model and is almost indistinguishable in the first and second ones. It is related to the differences in the site energies of the dimerized B820 pigments calculated with the charge layouts of three proposed models. The main contribution to the difference in these site energies of B820 BChls arises from the

dx.doi.org/10.1021/jp400239z | J. Phys. Chem. B XXXX, XXX, XXX−XXX

negatively charged ligand β-His31 (possibly this negative charge is effective and reflects some unusual charge redistribution) and histidine residue His37 (positively charged or neutral).

5. DISCUSSION

5.1. Spectral Deconvolution. Straightforward deconvolution of the LH3 experimental spectra, when the spectral region around 800 nm is initially ascribed to the B800 band, leads to a position of the upper excitonic component of the B820 band at ∼771 nm (see Figures 4 and 6). However, this result contradicts both the femtosecond transient absorption data and the microscopic modeling of the absorption spectrum. In the latter, the upper excitonic component appears completely overlapped with the B800 band, and this quantitatively agrees with the results of the deconvolution of LH3 spectra when part of the 800 nm absorption is initially attributed to B820 molecules. According to this conclusion, the high-frequency features in the LH3 absorption spectra are thus purely vibronic in their origin, which is consistent with their much weaker temperature dependence when compared with the main spectral bands (Figure 2).

As the temperature increases, the energy gap between the upper and lower Davydov subbands reduces from 573 to 503 cm^{-1} (Figure 6). Assuming the same scaling between the energy gap and the excitonic coupling in LH3 as that used for LH2 complexes,[19] the excitonic interaction of closely packed B820 BChls should decrease from 145 cm^{-1} at cryogenic temperatures to 127 cm^{-1} at room temperature. The former value is slightly lower than the one obtained from the microscopic simulations of the LH3 absorption spectrum (162−173 cm^{-1}; see Table 1) and almost 3 times smaller than that found for the LH2 complex.[19]

5.2. Microscopic Modeling. The modeled absorption spectra (Figure 8) are based on the available crystal structure of the LH3 complex.[32] Unfortunately, the crystal structure of LH3 and that of LH2 do not bear any indication on the protonation state of the aminoacid side chains nor on the H-bonds inside of these proteins. However, as was shown,[16] charged side chains of some amino acids within the proteins strongly influence the site energies of the pigments. Thus, the minor differences seen in the structures of the LH2[43] and LH3[32] complexes may actually induce large differences in the electrostatic environments of the complexes. On the other hand, resolution limitation of the structures obtained from crystallography may result in uncertainty at crucial details of the LH2/LH3 structure. For example, in the structural data file 2FKW.pdb of the LH2 complex,[51] the distances between coordinating Mg and N atoms within BChl−His complexes vary from 2.12 to 2.39 Å. Only one BChl−His complex out of the total 18 from the B850 ring displays the short 2.12 Å distance.[51] These structural data were obtained using the in meso crystallization method, resulting in denser packing of crystals. These distances within BChl−His complexes vary from 2.28 to 2.35 Å in the surfacto crystal[43] that we have used in our modeling of the LH2 spectra[16] and are equal to approximately 2.42 Å (with only one exception of 2.30 Å) in the data corresponding to the LH3 structure.[32] Thus, although the available structural data are crucial for microscopic modeling, it is questionable whether they can help to actually determine the essential parameters underlying the absorption properties of LH2 and LH3 complexes.

Solid-state nuclear magnetic resonance (NMR) experiments on LH2 complexes from *Rbl. acidophilus* showed that histidines that coordinate BChls molecules produce signals resembling ones from positively charged histidines.[52,53] As these ligands should be neutral or anionic for the stability of the BChl−His interaction, this observation was explained by charge redistribution from the coordinating BChl to the histidine in the overall neutral complex. The results of the modeling based on density functional theory reveal that this effect could be achieved only when performing calculations with the atomic coordinates of the BChl−His complex taken from the X-ray structure directly, without prior geometry optimization.[54] Upon geometry optimization, the distance between the nearest atoms of the BChl and histidine increases from 2.12 to 2.31 Å, and the effect almost disappears. This shows that these effects may be altered by the very small atomic displacements, obviously out of the precision of the available X-ray structures.

The NMR experiments showing both the signals of negatively charged (fully deprotonated) imidazoles ligated to Mg atoms of BChl *a*[42] and the signals resembling (though not equal to) the ones of positively charged histidines from the BChl−His complexes of the B850 ring of the LH2 complex[52,53] reveal the possibility of nontypical charges within the BChl−imidazole compounds. While searching for the charge layout within the LH3 complex that could reproduce the experimental absorption spectrum, we found that existence of some additional charge in the vicinity of the B820 (B850) pigments is necessary. Currently, in the model that we applied to calculate the elements of the Frenkel exciton Hamiltonian, only the full-charge protonation states of the titratable residues can be used. Therefore, fully deprotonated negative histidine ligands β-His31 were introduced in our calculations.

Our modeling of the LH3 absorption spectrum was performed at a single temperature of 100 K. The temperature enters our model as a parameter that tunes the spectral lineshape of the absorption spectrum. This can approximately take into account the vibrations causing the homogeneous portion of the linewidth. However, the static disorder may be influenced by the temperature as well[28] as it can reflect the temperature dependence of the protein charge configuration and protonation states. As mentioned above, minor differences of the protein configuration in the vicinity of the pigments can cause major effects on the charge redistribution within the BChl coordinating complex and thus directly influence the electronic properties of the pigment.

During microscopic modeling, we used the factor *f*, which scaled the ab initio calculated transition atomic partial charges[35] and defined the values of the interpigment excitonic couplings, obtained by utilizing the TrEsp method.[35] Because these excitonic couplings are proportional to f^2, even small variations of the scaling factor result in quite substantial differences in the modeled absorption spectra, as demonstrated in Figure 9. Moreover, it is noteworthy that the calculated dependence of the absorption spectrum on *f* qualitatively resembles the measured temperature dependence of these spectra (Figure 2). That means that the scaling factor *f* essentially encapsulates most of the *unresolved* structural features. What is more, the atomic partial charges of the BChl *a* molecules were calculated for the planar molecules,[35] while structural and spectroscopic data[41] indicate that BChl molecules are slightly distorted within the complexes. Thus, the scaling factor *f* may, to some degree, compensate for the possible drawback of using the partial charges calculated for the planar molecules.

Due to their different distortions, different position, and different charge distribution over their ligand histidines, the

dx.doi.org/10.1021/jp400239z | J. Phys. Chem. B XXXX, XXX, XXX−XXX

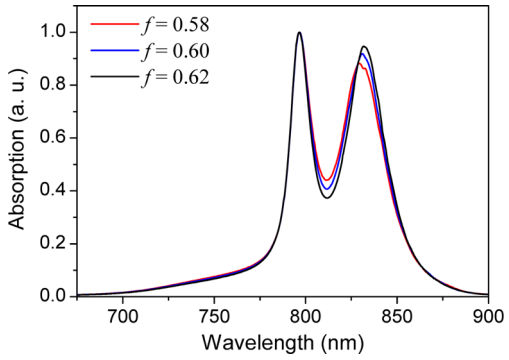

Figure 9. Calculated absorption spectrum of the LH3 complex at 100 K using different scaling factors *f* for transition atomic partial charges of BChls.

B820 (and B850) chromophores represent heterodimers rather than dimers. The distances between atoms of neighboring BChls are small; therefore, possible overlap of their wavefunctions must be taken into account while calculating the excitonic couplings, as was shown for the LH2 complex.[14] Some of these effects were examined using various theoretical approaches,[13,14,55−57] but the results are not unambiguous. In any case, the calculated values need to be adjusted to some experimental data. Consequently, in our model, the scaling factor *f* of the calculated atomic partial charges of BChl molecules[35] can stand for compensation of nonplanarity of the BChl molecules, changes in the excitonic couplings due to overlap of the wavefunctions of the closely positioned bacteriochlorin rings of the B820 pigments, ligating effects, and, probably, the partial charge redistribution at the axial ligand observed in NMR experiments. As was already mentioned, in our model, the effect of polarization of the environment is also incorporated into the same scaling factor. Therefore, any changes due to the polarizability of the environment might be also reflected in the value of the scaling factor *f*. Thus, even though the model of the absorption spectrum of LH3 is based on the available structural data, there are still many uncertainties presented. Nevertheless, we consider that our simple electrostatic model, which can be easily coordinated with the experiments by adjusting the tunable structural parameters, still allows us to determine the most important protein groups responsible for the tuning of the observed electronic spectra.

6. CONCLUSION

The modeling presented in this work leads to two major conclusions. First, the spectral properties of LH3 cannot be derived by simply changing the site energies of the B850 BChls in LH2 and keeping the other parameters constant. In LH3, a dramatic scaling of the BChl−BChl coupling in the densely packed ring has to be introduced to take into account the experimental data. Second, microscopic modeling of the LH3 complexes requires a change into the protonation state of one His residue to account for their spectroscopic properties. Part of these results could likely be taken into account by reconsidering the role of H-bonds between the acetyl carbonyl of the B820 molecules and the neighboring residues in LH2. Indeed, it has been shown that these H-bonds have a direct influence on the BChl site energies. They may also reduce the degrees of freedom of the B850 pigments, thus maintaining them in a configuration favoring their excitonic interactions. Breaking these H-bonds, which clearly increases the inhomogeneous broadening of the lower-energy transition of these complexes, may result in a larger dynamic disorder of the BChl dimer, which in turn could lead to a dramatic scaling of their excitonic interactions and reduce the influence of the electronic structure of their ligand.

■ ASSOCIATED CONTENT

Supporting Information

Matrix elements of the calculated LH3 single exciton Hamiltonian are presented in Table S1; Figure S1 shows the measured transient absorption kinetics of LH3; Figures S2 and S3 presents an explicit content of the self-modeling curve resolution procedures applied to the temperature-dependent absorption spectra of LH3. This material is available free of charge via the Internet at http://pubs.acs.org.

■ AUTHOR INFORMATION

Corresponding Author

*E-mail: leonas.valkunas@ff.vu.lt.

Notes

The authors declare no competing financial interest.

■ ACKNOWLEDGMENTS

This work was supported by the Research Council of Lithuania (LMT) through Grant No. 069/2012 (J.C., O.R., D.A., L.V.); the French Agence Nationale de la Recherché (ANR) through a Chaire d'excellence, ANR-07-CEX-009-01 (A.G.); the European Research Council (ERC) through an Advanced Grant Contract No. 267333 (B.R.); and the PHC-Gilbert programme (Campus France Contract No. 25543VJ) of the French Ministry for Foreign and European Affairs (MAEE) (B.R., L.V., E.S.).

■ REFERENCES

(1) van Grondelle, R.; Dekker, J. P.; Gillbro, T.; Sundstrom, V. Energy Transfer and Trapping in Photosynthesis. *Biochim. Biophys. Acta, Bioenerg.* **1994**, *1187*, 1−65.

(2) Bahatyrova, S.; Frese, R. N.; Siebert, C. A.; Olsen, J. D.; van der Werf, K. O.; van Grondelle, R.; Niederman, R. A.; Bullough, P. A.; Otto, C.; Hunter, C. N. The Native Architecture of a Photosynthetic Membrane. *Nature* **2004**, *430*, 1058−1062.

(3) McDermott, G.; Prince, S. M.; Freer, A. A.; Hawthornthwaite-Lawless, A. M.; Papiz, M. Z.; Cogdell, R. J.; Isaacs, N. W. Crystal-Structure of an Integral Membrane Light-Harvesting Complex from Photosynthetic Bacteria. *Nature* **1995**, *374*, 517−521.

(4) van Amerongen, H.; Valkunas, L.; van Grondelle, R. *Photosynthetic Excitons*; World Scientific: Singapore, 2000.

(5) Urboniene, V.; Vrublevskaja, O.; Gall, A.; Trinkunas, G.; Robert, B.; Valkunas, L. Temperature Broadening of LH2 Absorption in Glycerol Solution. *Photosynth. Res.* **2005**, *86*, 49−59.

(6) Vrublevskaja, O.; Urboniene, V.; Trinkunas, G.; Valkunas, L.; Gall, A.; Robert, B. Estimation of the Spectral Density Function of LH2 Complexes from the Temperature Dependence of the Absorption Spectra. *Lith. J. Phys.* **2006**, *46*, 39−46.

(7) Urboniene, V.; Vrublevskaja, O.; Trinkunas, G.; Gall, A.; Robert, B.; Valkunas, L. Solvation Effect of Bacteriochlorophyll Excitons in Light-Harvesting Complex LH2. *Biophys. J.* **2007**, *93*, 2188−2198.

(8) van Grondelle, R.; Novoderezhkin, V. I. Energy Transfer in Photosynthesis: Experimental Insights and Quantitative Models. *Phys. Chem. Chem. Phys.* **2006**, *8*, 793−807.

(9) Abramavicius, D.; Valkunas, L.; van Grondelle, R. Exciton Dynamics in Ring-Like Photosynthetic Light-Harvesting Complexes: A Hopping Model. *Phys. Chem. Chem. Phys.* **2004**, *6*, 3097−3105.

(10) Freiberg, A.; Timpmann, K.; Ruus, R.; Woodbury, N. W. Disordered Exciton Analysis of Linear and Nonlinear Absorption Spectra of Antenna Bacteriochlorophyll Aggregates: LH2-Only Mutant Chromatophores of *Rhodobacter sphaeroides* at 8 K under Spectrally Selective Excitation. *J. Phys. Chem. B* **1999**, *103*, 10032−10041.
(11) Freiberg, A.; Ratsep, M.; Timpmann, K.; Trinkunas, G.; Woodbury, N. W. Self-Trapped Excitons in LH2 Antenna Complexes between 5 K and Ambient Temperature. *J. Phys. Chem. B* **2003**, *107*, 11510−11519.
(12) Wu, H. M.; Reddy, N. R. S.; Small, G. J. Direct Observation and Hole Burning of the Lowest Exciton Level (B870) of the LH2 Antenna Complex of *Rhodopseudomonas acidophila* (strain 10050). *J. Phys. Chem. B* **1997**, *101*, 651−656.
(13) Krueger, B. P.; Scholes, G. D.; Fleming, G. R. Calculation of Couplings and Energy-Transfer Pathways between the Pigments of LH2 by the Ab Initio Transition Density Cube Method. *J. Phys. Chem. B* **1998**, *102*, 5378−5386.
(14) Scholes, G. D.; Gould, I. R.; Cogdell, R. J.; Fleming, G. R. Ab Initio Molecular Orbital Calculations of Electronic Couplings in the LH2 Bacterial Light-Harvesting Complex of *Rps. Acidophila*. *J. Phys. Chem. B* **1999**, *103*, 2543−2553.
(15) Tretiak, S.; Middleton, C.; Chernyak, V.; Mukamel, S. Bacteriochlorophyll and Carotenoid Excitonic Couplings in the LH2 System of Purple Bacteria. *J. Phys. Chem. B* **2000**, *104*, 9540−9553.
(16) Rancova, O.; Sulskus, J.; Abramavicius, D. Insight into the Structure of Photosynthetic LH2 Aggregate from Spectroscopy Simulations. *J. Phys. Chem. B* **2012**, *116*, 7803−7814.
(17) Cogdell, R. J.; Gall, A.; Kohler, J. The Architecture and Function of the Light-Harvesting Apparatus of Purple Bacteria: from Single Molecules to In Vivo Membranes. *Q. Rev. Biophys.* **2006**, *39*, 227−324.
(18) Ketelaars, M.; van Oijen, A. M.; Matsushita, M.; Kohler, J.; Schmidt, J.; Aartsma, T. J. Spectroscopy on the B850 Band of Individual Light-Harvesting 2 Complexes of *Rhodopseudomonas Acidophila* I. Experiments and Monte Carlo Simulations. *Biophys. J.* **2001**, *80*, 1591−1603.
(19) Trinkunas, G.; Zerlauskiene, O.; Urboniene, V.; Chmeliov, J.; Gall, A.; Robert, B.; Valkunas, L. Exciton Band Structure in Bacterial Peripheral Light-Harvesting Complexes. *J. Phys. Chem. B* **2012**, *116*, 5192−5198.
(20) Cogdell, R. J.; Durant, I.; Valentine, J.; Lindsay, J. G.; Schmidt, K. The Isolation and Partial Characterisation of the Light-Harvesting Pigment-Protein Complement of *Rhodopseudomonas acidophila*. *Biochim. Biophys. Acta, Bioenerg.* **1983**, *722*, 427−435.
(21) Angerhofer, A.; Cogdell, R. J.; Hipkins, M. F. A Spectral Characterisation of the Light-Harvesting Pigment−Protein Complexes from *Rhodopseudomonas acidophila*. *Biochim. Biophys. Acta, Bioenerg.* **1986**, *848*, 333−341.
(22) Gardiner, A. T.; Cogdell, R. J.; Takaichi, S. The Effect of Growth-Conditions on the Light-Harvesting Apparatus in *Rhodopseudomonas acidophila*. *Photosynth. Res.* **1993**, *38*, 159−167.
(23) Zuber, H.; Brunisholz, R. A. Structure and Function of Antenna Polypeptides and Chlorophyll−Protein Complexes: Principles and Variability. In *Chlorophylls*; Scheer, H., Ed.; CRC Press: Boca Raton, FL, 1991; pp 627−703.
(24) Fowler, G. J. S.; Visschers, R. W.; Grief, G. G.; Vangrondelle, R.; Hunter, C. N. Genetically Modified Photosynthetic Antenna Complexes with Blueshifted Absorbency Bands. *Nature* **1992**, *355*, 848−850.
(25) Firsow, N. N.; Drews, G. Differentiation of the Intracytoplasmic Membrane of *Rhodopseudomonas palustris* Induced by Variations of Oxygen Partial Pressure or Light Intensity. *Arch. Microbiol.* **1977**, *115*, 299−306.
(26) Gall, A.; Robert, B. Characterization of the Different Peripheral Light-Harvesting Complexes from High- and Low-Light Grown Cells from *Rhodopseudomonas palustris*. *Biochemistry* **1999**, *38*, 5185−5190.
(27) Gall, A.; Sogaila, E.; Gulbinas, V.; Ilioaia, O.; Robert, B.; Valkunas, L. Spectral Dependence of Energy Transfer in Wild-Type Peripheral Light-Harvesting Complexes of Photosynthetic Bacteria. *Biochim. Biophys. Acta, Bioenerg.* **2010**, *1797*, 1465−1469.
(28) Zerlauskiene, O.; Trinkunas, G.; Gall, A.; Robert, B.; Urboniene, V.; Valkunas, L. Static and Dynamic Protein Impact on Electronic Properties of Light-Harvesting Complex LH2. *J. Phys. Chem. B* **2008**, *112*, 15883−15892.
(29) Abramavicius, D.; Palmieri, B.; Mukamel, S. Extracting Single and Two-Exciton Couplings in Photosynthetic Complexes by Coherent Two-Dimensional Electronic Spectra. *Chem. Phys.* **2009**, *357*, 79−84.
(30) Abramavicius, D.; Palmieri, B.; Voronine, D. V.; Sanda, F.; Mukamel, S. Coherent Multidimensional Optical Spectroscopy of Excitons in Molecular Aggregates; Quasiparticle versus Supermolecule Perspectives. *Chem. Rev.* **2009**, *109*, 2350−2408.
(31) May, V.; Kühn, O. *Charge and Energy Transfer Dynamics in Molecular Systems*, 3rd, rev. and enl. ed.; Wiley-VCH: Weinheim, Germany, 2011.
(32) McLuskey, K.; Prince, S. M.; Cogdell, R. J.; Isaacs, N. W. The Crystallographic Structure of the B800−820 LH3 Light-Harvesting Complex from the Purple Bacteria *Rhodopseudomonas acidophila* Strain 7050. *Biochemistry* **2001**, *40*, 8783−8789.
(33) Adolphs, J.; Renger, T. How Proteins Trigger Excitation Energy Transfer in the FMO Complex of Green Sulfur Bacteria. *Biophys. J.* **2006**, *91*, 2778−2797.
(34) Adolphs, J.; Muh, F.; Madjet, M. E. A.; Renger, T. Calculation of Pigment Transition Energies in the FMO Protein. *Photosynth. Res.* **2008**, *95*, 197−209.
(35) Madjet, M. E.; Abdurahman, A.; Renger, T. Intermolecular Coulomb Couplings from Ab Initio Electrostatic Potentials: Application to Optical Transitions of Strongly Coupled Pigments in Photosynthetic Antennae and Reaction Centers. *J. Phys. Chem. B* **2006**, *110*, 17268−17281.
(36) Muh, F.; Madjet, M. E. A.; Adolphs, J.; Abdurahman, A.; Rabenstein, B.; Ishikita, H.; Knapp, E. W.; Renger, T. α-Helices Direct Excitation Energy Flow in the Fenna−Matthews−Olson Protein. *Proc. Natl. Acad. Sci. U.S.A.* **2007**, *104*, 16862−16867.
(37) Renger, T. Theory of Excitation Energy Transfer: From Structure to Function. *Photosynth. Res.* **2009**, *102*, 471−485.
(38) Adolphs, J.; Muh, F.; Madjet, M. E. A.; Busch, M. S. A.; Renger, T. Structure-Based Calculations of Optical Spectra of Photosystem I Suggest an Asymmetric Light-Harvesting Process. *J. Am. Chem. Soc.* **2010**, *132*, 3331−3343.
(39) Fowler, G. J. S.; Sockalingum, G. D.; Robert, B.; Hunter, C. N. Blue Shifts in Bacteriochlorophyll Absorbency Correlate with Changed Hydrogen-Bonding Patterns in Light-Harvesting 2 Mutants of *Rhodobacter Sphaeroides* with Alterations at α-Tyr-44 and α-Tyr-45. *Biochem. J.* **1994**, *299*, 695−700.
(40) Sturgis, J. N.; Jirsakova, V.; Reisshusson, F.; Cogdell, R. J.; Robert, B. Structure and Properties of the Bacteriochlorophyll Binding-Site in Peripheral Light-Harvesting Complexes of Purple Bacteria. *Biochemistry* **1995**, *34*, 517−523.
(41) Gall, A.; Fowler, G. J. S.; Hunter, C. N.; Robert, B. Influence of the Protein Binding Site on the Absorption Properties of the Monomeric Bacteriochlorophyll in *Rhodobacter sphaeroides* LH2 Complex. *Biochemistry* **1997**, *36*, 16282−16287.
(42) Alia; Matysik, J.; Erkelens, C.; Hulsbergen, F. B.; Gast, P.; Lugtenburg, J.; de Groot, H. J. M. Bacteriochlorophyll/Imidazole and Chlorophyll/Imidazole Complexes are Negatively Charged in an Apolar Environment. *Chem. Phys. Lett.* **2000**, *330*, 325−330.
(43) Papiz, M. Z.; Prince, S. M.; Howard, T.; Cogdell, R. J.; Isaacs, N. W. The Structure and Thermal Motion of the B800−850 LH2 Complex from *Rps. acidophila* at 2.0 Å Resolution and 100 K: New Structural Features and Functionally Relevant Motions. *J. Mol. Biol.* **2003**, *326*, 1523−1538.
(44) Humphrey, W.; Dalke, A.; Schulten, K. VMD: Visual Molecular Dynamics. *J. Mol. Graph. Modell.* **1996**, *14*, 33−38.
(45) Knox, R. S.; Spring, B. Q. Dipole Strengths in the Chlorophylls. *Photochem. Photobiol.* **2003**, *77*, 497−501.
(46) Alden, R. G.; Johnson, E.; Nagarajan, V.; Parson, W. W.; Law, C. J.; Cogdell, R. G. Calculations of Spectroscopic Properties of the LH2

Bacteriochlorophyll−Protein Antenna Complex from *Rhodopseudomonas acidophila*. *J. Phys. Chem. B* **1997**, *101*, 4667−4680.
(47) Abramavicius, D.; Butkus, V.; Valkunas, L. Quantum Dynamics and Spectroscopy of Excitons in Molecular Aggregates. In *Quantum Efficiency in Complex Systems. Part II, From Molecular Aggregates to Organic Solar Cells*; Würfel, U., Thorwart, M., Weber, E. R., Eds.; Elsevier Academic Press: San Diego, CA; London, 2011; pp 3−46.
(48) Jang, S.; Newton, M. D.; Silbey, R. J. Multichromophoric Förster Resonance Energy Transfer from B800 to B850 in the Light Harvesting Complex 2: Evidence for Subtle Energetic Optimization by Purple Bacteria. *J. Phys. Chem. B* **2007**, *111*, 6807−6814.
(49) Olbrich, C.; Kleinekathofer, U. Time-Dependent Atomistic View on the Electronic Relaxation in Light-Harvesting System II. *J. Phys. Chem. B* **2010**, *114*, 12427−12437.
(50) Butkus, V.; Valkunas, L.; Abramavicius, D. Molecular Vibrations-Induced Quantum Beats in Two-Dimensional Electronic Spectroscopy. *J. Chem. Phys.* **2012**, 137.
(51) Cherezov, V.; Clogston, J.; Papiz, M. Z.; Caffrey, M. Room to Move: Crystallizing Membrane proteins in Swollen Lipidic Mesophases. *J. Mol. Biol.* **2006**, *357*, 1605−1618.
(52) Alia; Matysik, J.; Soede-Huijbregts, C.; Baldus, M.; Raap, J.; Lugtenburg, J.; Gast, P.; van Gorkom, H. J.; Hoff, A. J.; de Groot, H. J. M. Ultrahigh Field MAS NMR Dipolar Correlation Spectroscopy of the Histidine Residues in Light-Harvesting Complex II from Photosynthetic Bacteria Reveals partial Internal Charge Transfer in the B850/His Complex. *J. Am. Chem. Soc.* **2001**, *123*, 4803−4809.
(53) Alia; Matysik, J.; de Boer, I.; Gast, P.; van Gorkom, H. J.; de Groot, H. J. M. Heteronuclear 2D (^{1}H−^{13}C) MAS NMR Resolves the Electronic Structure of Coordinated Histidines in Light-Harvesting Complex II: Assessment of Charge Transfer and Electronic Delocalization Effect. *J. Biomol. NMR* **2004**, *28*, 157−164.
(54) Wawrzyniak, P. K.; Alia, A.; Schaap, R. G.; Heemskerk, M. M.; de Groot, H. J. M.; Buda, F. Protein-Induced Geometric Constraints and Charge Transfer in Bacteriochlorophyll−histidine Complexes in LH2. *Phys. Chem. Chem. Phys.* **2008**, *10*, 6971−6978.
(55) He, Z.; Sundstrom, V.; Pullerits, T. Influence of the Protein Binding Site on the Excited States of Bacteriochlorophyll: DFT Calculations of B800 in LH2. *J. Phys. Chem. B* **2002**, *106*, 11606−11612.
(56) Neugebauer, J. Photophysical Properties of Natural Light-Harvesting Complexes Studied by Subsystem Density Functional Theory. *J. Phys. Chem. B* **2008**, *112*, 2207−2217.
(57) Konig, C.; Neugebauer, J. Quantum Chemical Description of Absorption Properties and Excited-State Processes in Photosynthetic Systems. *ChemPhysChem* **2012**, *13*, 386−425.